Cellular Signalling 62 (2019) 109330

Contents lists available at ScienceDirect

Cellular Signalling

journal homepage: www.elsevier.com/locate/cellsig

ROS-mediated relationships between metabolism and DAF-16 subcellular localization in *Caenorhabditis elegans* revealed by a novel fluorometric method

Martha N. Mendelski, Alex Keshet, Nadine Hoffschröer, Thiago Strieder, Sarah A. Winter, Rüdiger J. Paul*

Institute of Zoophysiology, WWU Münster, Münster, Germany

ARTICLE INFO

Keywords:
AAK-2/AMPK
DAF-16/FoxO
Hypoxia
LET-363/TOR
Redox

ABSTRACT

Signalling pathways provide a fine-tuned control network for catabolic and anabolic cellular processes under changing environmental conditions (e.g. changes in oxygen partial pressure, Po_2). These pathways frequently activate or deactivate transcription factors (TFs) in the cytoplasm, with the subsequent nuclear translocation of activated TFs constituting a prerequisite for gene control and expression. This study introduces a newly developed fluorometric method for the quantification of relationships between environmental factors and the subcellular localization of reporter-coupled TFs in *Caenorhabditis elegans* (and possibly other transparent organisms). We applied this method to determine and analyse the relationship between Po_2 and the subcellular localization of the GFP-coupled transcription factor DAF-16 (FoxO) of the DAF-2 (insulin/IGF-1) signalling pathway via the DAF-16::GFP fluorescence intensity of whole worms (Po_2 characteristic). The Po_2 characteristic resembled the Po_2-specific metabolic rate of *C. elegans*, with a critical Po_2 (P_co_2) of 3.6 kPa separating two Po_2 ranges, where either anaerobic metabolism and DAF-16::GFP nuclear occupancy strongly increased (i.e. decreasing DAF-16::GFP fluorescence intensity) ($Po_2 < P_co_2$) or aerobic metabolism and DAF-16::GFP cytoplasmic localization prevailed ($Po_2 > P_co_2$). These results and other data, which included the Po_2-specific mitochondrial oxidation-reduction state of whole worms (as determined using the endogenous NADH fluorescence) and the effects of higher levels of reactive oxygen species (ROS) or RNAi-mediated knockdowns of catabolic or anabolic control genes (*aak-2* or *let-363*) on the Po_2 characteristic, suggest that ROS play a decisive role for DAF-16 nuclear translocation due to tissue hypoxia or higher anabolic activity induced by *aak-2(RNAi)*. As DAF-16 and its target genes are of central importance for the cellular stress resistance, ROS-mediated relationships between metabolism and DAF-16 subcellular (i.e. nuclear) localization provide protection of the cell machinery against elevated ROS formation under challenging metabolic conditions.

1. Introduction

The complex interplay between catabolic and anabolic processes requires a fine-tuned control network, which includes signalling proteins and pathways such as the AMP-activated protein kinase (AMPK) and the target of rapamycin (TOR) signalling pathway. AMPK is a sensor of low energy levels and interacts with different signalling pathways [1]. A high AMP:ATP ratio activates, for instance, the *C. elegans* AMPK α subunit AAK-2 [2], which stimulates catabolic (ATP-producing) processes (e.g. fatty acid oxidation) and downregulates anabolic (ATP-consuming) processes (e.g. protein biosynthesis and growth) [3]. TOR complex 1 (TORC1) signalling [4], with LET-363 (CeTor) and DAF-15 (Raptor) as key components of TORC1 in *C. elegans*, uses signals related to the nutrient stores, oxygen supply, or

Abbreviations: AAK-2, AMP-activated kinase 2; AMPK, AMP-activated protein kinase; CeTor, *C. elegans* TOR; DAF-2, DAF-15, DAF-16, abnormal dauer formation 2, 15, 16; FoxO, forkhead box O; GFP, green fluorescent protein; IGF-1, insulin-like growth factor 1; JNK-1, jun N-terminal kinase 1; λ_{ex}, λ_{em}, excitation and emission wavelength; LET-363, lethal 363 (ortholog of human mechanistic TOR, mTOR); MAP kinase, mitogen-activated protein kinase; Po_2, oxygen partial pressure; P_co_2, critical Po_2; RNAi, RNA interference; ROS, reactive oxygen species; SIR, sirtuin; SOD-3, superoxide dismutase 3; TOR, target of rapamycin; TORC1, TOR complex 1; TF, transcription factor

* Corresponding author at: Institute of Zoophysiology, University of Münster (WWU), Schlossplatz 8, 48143 Münster, Germany.
E-mail addresses: m_mend08@uni-muenster.de (M.N. Mendelski), n.hoffschroeer@uni-muenster.de (N. Hoffschröer), zoophys@uni-muenster.de (T. Strieder), swint_01@uni-muenster.de (S.A. Winter), paulr@uni-muenster.de (R.J. Paul).

https://doi.org/10.1016/j.cellsig.2019.05.015
Received 13 March 2019; Received in revised form 27 May 2019; Accepted 28 May 2019
Available online 29 May 2019
0898-6568/

energy state of the cells to control anabolic processes in a positive and autophagy in a negative manner [5]. Amino acid deficiency, hypoxia, or activated AMPK inhibit TORC1 signalling, which causes autophagic degradation. S6K1 kinase, a downstream target of TORC1 signalling, likely represses AMPK signalling [6].

Signalling pathways frequently activate or deactivate transcription factors (TFs), with their nuclear translocation constituting a prerequisite for TF-specific gene control. In case of insulin/IGF-1 signalling (IIS; DAF-2 signalling in *C. elegans*) [7], environmental signals cause secretion of different insulin-like peptides (for instance, from chemosensory neurons) [8], which can activate or inhibit DAF-2 signalling after their binding to the DAF-2 receptor [9]. Activated DAF-2 signalling results in a site-specific phosphorylation of the transcription factor DAF-16/FoxO, which causes its retention in the cytoplasm [10]. Several environmental cues (e.g. heat, hypoxia, starvation, or oxidative stress due to juglone or paraquat treatment) result in a deactivation of DAF-2 signalling and a higher DAF-16 nuclear occupancy, which can be visualized in *C. elegans* strains carrying a *daf-16*::*gfp* transgene [11–13]. The subcellular localization of reporter-coupled TFs (e.g. DAF-16::GFP) has hitherto been evaluated by a classification between two or three categories (e.g. cytoplasmic, intermediate, or nuclear localization of the fluorescent fusion protein) [14]. Nuclear DAF-16 influences, positively or negatively, the expression of several hundred genes [15], including *sod-3* encoding a mitochondrial manganese superoxide dismutase [16] or *daf-15* encoding the *C. elegans* orthologue of Raptor [17]. Upregulated *sod-3* expression, for instance, promotes stress resistance and longevity [18]. DAF-2 signalling and other signalling proteins and pathways can act in opposing directions [1]. Whereas activated DAF-2 signalling inhibits the nuclear translocation and activity of DAF-16, activated AMPK promotes DAF-16-mediated gene expression, however, without affecting the subcellular localization of this TF [19,20]. TORC1 signalling (and/or translation initiation) in turn inhibit the nuclear translocation and activity of DAF-16 [21].

As the subcellular localization of TFs provides important information about a possible TF-specific gene control, a novel fluorometric method was developed and thoroughly tested, which allows quantification of the relationships between environmental factors (e.g. Po_2) and the subcellular localization of reporter-coupled TFs (e.g. DAF-16::GFP) in transparent whole organisms. The determination of the exact shape of these relationships is the precondition for comparative analyses with other cellular processes that are controlled by a specific environmental factor or between different environmental factors that affect the subcellular localization of a specific TF. As oxygen availability (hypoxia) strongly affects cellular signalling and metabolism (see above), we applied this new method in *C. elegans* to quantify the relationship between Po_2 and DAF-16::GFP subcellular localization (Po_2 characteristic). The similarity in shape of this Po_2 characteristic and the Po_2-specific aerobic metabolic rate of these animals prompted us to perform additional measurements on the Po_2-specific mitochondrial redox state. RNA interference (RNAi) experiments were also conducted on metabolic control genes (*aak-2* or *let-363*) to study the consequences of a more strongly or weakly activated anabolism on the Po_2 characteristic and the Po_2-specific mitochondrial redox state. As increases in the production and level of reactive oxygen species (ROS) were plausible explanations for the higher DAF-16::GFP nuclear occupancy under severe hypoxia or due to *aak-2(RNAi)*, the effects of different H_2O_2 concentrations on the Po_2 characteristic were determined, which provided further evidence for positive effects of ROS on DAF-16::GFP nuclear occupancy.

2. Methods

2.1. Animals

C. elegans N2 Bristol variety (wild type, WT) and the transgenic TJ356 strain that carries a genome-integrated *daf-16*::*gfp* construct (zIs356 IV) were obtained from the Caenorhabditis Genetics Center (CGC; https://cgc.umn.edu/). Worms were maintained at 20 °C on nematode growth medium (NGM) plates with *E. coli* OP50 as food source.

2.2. RNA interference

For *aak-2* (T01C8.1) knockdown by RNA interference (RNAi), double-stranded RNA (dsRNA) was applied to TJ356 by feeding with the *E. coli* HT115(DE3) clone X-7D05 from Source BioScience LifeSciences (Berlin, Germany). The *E. coli* HT115(DE3)/pL4440 clone, which carries the empty vector, was fed to control worms. The *E. coli* HT115(DE3) clone for *let-363* (B0261.2) RNAi was generated in our laboratory by cloning a fragment of the *let-363* genomic sequence (primer forward: 5′-GGTATCTATCTCATCGTGTGCT-3′; primer reverse: 5′-TTTGGGTTGCTGACTATGTG-3′; amplicon size: 246 bp) into the L4440 vector and transforming the *E. coli* strain. Identity of the bacteria was checked by sequencing. Bacteria were grown overnight at 37 °C in lysogeny broth (LB) medium containing 100 μg/mL ampicillin. NGM plates with isopropyl β-D-1-thiogalactopyranoside (IPTG; 1 mmol/L) were seeded with 1 mL of bacterial suspension (OD_{600} = 1) and kept for 24 h at 20 °C to induce dsRNA expression. Synchronized L1 larvae [22] were transferred to these plates, grown until the adult stage, and then used for experimentation. Feeding other worms with HT115(DE3)/pL4440, *dpy-7* [F46C8.6], which induces the *dumpy* phenotype, served as a control for the effect of IPTG.

2.3. Preparation of worms for the measurement of DAF-16::GFP and NADH fluorescence intensities

Control or RNAi-treated synchronized adult TJ356 worms, with control worms fed with *E. coli* HT115, were washed from their NGM plates with M9 buffer [23] and collected in Eppendorf tubes with a rounded base (volume: 2 mL). After the worms had sunk to the tube base, the buffer above them was replaced several times to obtain a clear supernatant. Subsequent centrifugation (2700 xg, 1 min, 20 °C) resulted in pellets of agar residues and bacteria attached to the tube wall, with the worms localized at the tube base. Worms and supernatant were transferred to a new tube, and after re-centrifugation, the worm-free supernatant was removed. As any bacterial fluorescence did not interfere with DAF-16::GFP fluorescence (see Results), the respective animals were provided with food during measurements by adding 3–5 μL of *E. coli* OP50 suspension (OD_{600} = 1.2). For the NADH fluorescence measurements, however, the worms were transferred to bacteria-free NGM plates for 30 min of defecation to exclude or at least minimize contributions by bacterial fluorescence. These worms were then washed off the plates, cleaned, and concentrated as described. For H_2O_2 treatments, the worm pellet was resuspended in up to 500 μL of a freshly prepared H_2O_2 solution (H_2O_2 dissolved in M9 buffer; 0.02 or 1 mmol/L H_2O_2) and, after a good mixing, centrifuged for 3 s. In this case, the residual volume of the supernatant was kept larger to ensure effectiveness of the treatment.

A small droplet (5 μL) of worm suspension (with or without bacteria) was then transferred to a small container (i.e. a single micro well cut out from a standard 96-well plate; Brand*plates*®, pureGrade™, BrandTech Scientific, Essex, CT). The remaining buffer was removed by pipette, and another droplet of worm suspension was applied. This procedure was repeated until 150–200 worms were at the bottom of the micro well (sufficiently covered with buffer), which was placed on the floor of a thermostated animal chamber (containing a thin 1–2-mm water layer to prevent desiccation of the droplet) for microscopy [24]. To avoid trapped air bubbles in the cavity below the micro well, it was filled with water. For the NADH fluorescence measurements, residual fluorescent fibers were removed with a needle. The chamber was then closed by screwing its transparent cover. Water from a laboratory water bath served to control the temperature of the chamber, which was also measured using a needle-type thermal sensor within the chamber [24].

Gas mixtures of normocapnic nitrogen and air supplied by a Wösthoff gas-mixing pump were vapour-saturated using humidifiers and partially fed into the entry port of the chamber. Gas leaving the chamber was bubbled through a water-filled vessel to control the chamber's tightness. Fluorescence measurements under changing oxygen conditions were carried out at $T = 20\,^{\circ}C$.

2.4. Experimental setup and protocol for the measurement of DAF-16::GFP and NADH fluorescence intensities

A previously described setup for "optophysiological measurements [25] was re-used for the DAF-16::GFP and endogenous NADH fluorescence assays. Briefly, an inverted fluorescence microscope (Axiovert 100; Zeiss, Germany) was equipped with a computer-controlled monochromator (T.I.L.L. Photonics, Planegg, Germany) as a light source and a photomultiplier (H5784; Hamamatsu Photonics, Herrsching, Germany) for fluorescence detection. Filter settings were $\lambda_{ex} = 460$ nm and $\lambda_{em} > 520$ nm for the DAF-16::GFP fluorescence assay and $\lambda_{ex} = 350$ nm and $\lambda_{em} > 420$ nm for the NADH fluorescence assay. A self-written Visual Basic program (VB 2010; Microsoft) on a PC controlled the monochromator via a 12-bit digital-analog converter and recorded the data from the photomultiplier via a 12-bit analog-to-digital converter. To minimize light exposure, the monochromator was triggered to emit the excitation wavelength every 20 s for only 5 s, during which data were recorded at maximum speed, averaged, and saved.

After focusing the worms in the micro well under white light (using an objective with a magnification of 2.5× for GFP or 5× for NADH measurements), with the image of the droplet covering an area smaller than the viewing range of the eyepiece and the incidence range of the photomultiplier, measurements were initiated by setting up the microscope (fluorescence mode) and photomultiplier (amplification). After a period of 20 min under air provision to check for a steady signal, a sequence of different gas-mixtures was applied and the photomultiplier signal recorded, with the gas-mixing pump set to a new mixing ratio after the fluorescence signal had reached a plateau. Other experiments involved the application of different temperatures under normoxia. After the experiments, worms and droplet were checked under white light for unabated mobility and buffer volume.

2.5. Control experiments to exclude decreases in DAF-16::GFP concentration during short-term heat exposures

After taking fluorescence images ($\lambda_{ex} = 460$ nm, $\lambda_{em} > 520$ nm) of six living TJ356 worms at 20 °C, three worms each were incubated at 20 °C or 37 °C for 10 min, quickly frozen (−80 °C) and thawed again, before further fluorescence images of these worms were taken under unchanged recording conditions. After another 30 min under unchanged temperature conditions (20 °C), further fluorescence images of these worms were taken. The DAF-16::GFP fluorescence intensities of these worms were then determined using the fluorescence images and ImageJ [26]. In a next experimental series, 4 batches of synchronized adult TJ356 worms were generated. Then, 4 aliquots per batch and temperature, with each aliquot containing several hundred worms, were incubated at 20 °C, 30 °C, or 34 °C for 30 min and quickly frozen in liquid nitrogen. After adding 300 µL of extraction buffer (10 mmol/L HEPES, 5 mmol/L $MgCl_2$, 200 mol/L NaCl, 10% glycerol plus cOmplete™ Mini protease inhibitor cocktail, pH 7.1) to each aliquot, they were thawed, homogenized twice (for 2 min each) within a 60-min period on ice using pellet pestles (Pellet pestles, blue polypropylene, Kimble®/Kontes, Sigma-Aldrich), and centrifuged (20,800 x*g*, 20 min; 4 °C), with the soluble proteins in the supernatant used for the subsequent measurements. The DAF-16::GFP fluorescence intensity ($\lambda_{ex} = 460$ nm, $\lambda_{em} > 520$ nm) or protein concentration of duplicate samples of the 48 aliquots were determined using a multimode microplate reader (TriStar LB 941; Berthold Technologies, Bad Wildbad, Germany) or the Bradford test [27].

2.6. Development studies

Synchronized adult TJ365 worms were transferred to control, *aak-2(RNAi)*, or *let-363(RNAi)* plates (see above). The worms were allowed to lay eggs for 1.5 h. Then, the adult worms were removed from the plates (starting time of the experiments: 0 h). Air (normoxia) or a mixture of 70% normocapnic nitrogen and 30% air (hypoxia) supplied by a Wösthoff gas-mixing pump (Bochum, Germany) were vapour-saturated using humidifiers and fed into a hermetically sealed chamber (equipped with a clip-lock), into which the plates were placed. Gas leaving the chamber was bubbled through a water-filled vessel to control the chamber's tightness. The incubation temperature was 20 °C. To withdraw a plate, the chamber was briefly opened and then rapidly resealed. The developmental stages (L1, L2, L3, L4 larval stages and adults) of the worms on a plate were determined 38–48 h, 62–72 h, and 86–96 h (every 2 h) after the starting time by visual observation and counting.

2.7. Real-time PCR

Synchronized adult TJ356 control, *aak-2(RNAi)*-, or *let-363(RNAi)*-treated worms were incubated for 3 h under hypoxia ($Po_2 = 6.3$ kPa) or normoxia. The worms were then washed from their plates with purified water and cleaned of bacteria by at least two washing steps (see above) using purified water. Approximately 500 µL of worm suspension was then quickly frozen in liquid nitrogen and stored at −80 °C. After thawing and centrifugation (17,900 x *g*, 2 min, 20 °C), the pellet was used for total RNA extraction (peqGOLD Total RNA Kit, Safety-Line, which includes a PerfectBind RNA binding and DNA removing column; PEQLAB Biotechnologie, Erlangen, Germany). After addition of 200 µL of lysis solution from the kit and homogenization using pellet pestles (Pellet pestles, blue polypropylene, Kimble®/Kontes, Sigma-Aldrich), another 200 µL of lysis solution was added. After a short incubation period (2–3 min), RNA extracts were collected according to the instructions provided with the kit. RNA concentrations were measured using a NanoDrop™ spectrophotometer (Thermo Fisher Scientific, Waltham, MA). cDNA was synthesized from total RNA (300 ng, adjusted according to the respective RNA concentration) via reverse transcription (RevertAid First Strand cDNA Synthesis Kit; Thermo Fisher Scientific) according to the manufacturer's protocol. Primers for the quantitative RT-qPCR and associated gene-specific standards were designed using the PerlPrimer program [28], with the setting that primers should span intron/exon boundaries. The optimum annealing temperatures given by the program were checked by gradient PCR. The following primers were used for *sod-3* (forward primer: 5′-AGCACACT CTCCCAGATCTC-3′; reverse primer: 5′-CGAAGTCGCGCTTAATA GTG-3′; amplicon size 299 bp) or *cdc-42* (forward primer: 5′-TTCGAC AATTACGCCGTCAC-3′; reverse primer: 5′-CCTGAGATCGACTTGAGT ACC-3′; amplicon size 251 bp). Gene-specific standards were prepared by semi-quantitative RT-sqPCR (TPersonal thermocycler; Biometra, Göttingen, Germany) (reaction: 3 min at 95 °C, 45 s at 95 °C, 20 s at 60 °C, 30 s at 71 °C; 35 cycles). The produced DNA quantities were measured using a NanoDrop spectrophotometer. A concentration series was prepared using purified water with ten-fold dilution steps. RT-qPCR was carried out using a Real-Time PCR System (Eco Real-Time PCR; Illumina, San Diego, CA) and the SYBR *Premix Ex Taq* (Tli RNase H Plus) kit (Takara Bio Europe, Saint-Germain-en-Laye, France), with 12 min at 95 °C, followed by 10 s at 95 °C, and 30 s at 60 °C (40 cycles). A melting curve was then generated (15 s at 95 °C, 30 s at 60 °C, 15 s at 95 °C). Each reaction contained 1 µL of template cDNA, 5 µL of SYBR *Premix*, 0.5 µL of each primer and 3 µL of purified water, resulting in a final volume of 10 µL. To calculate the mRNA levels, the software provided with the RT-qPCR system was used, and relative *sod-3* mRNA levels were determined as ratios between the mRNA levels of *sod-3* and

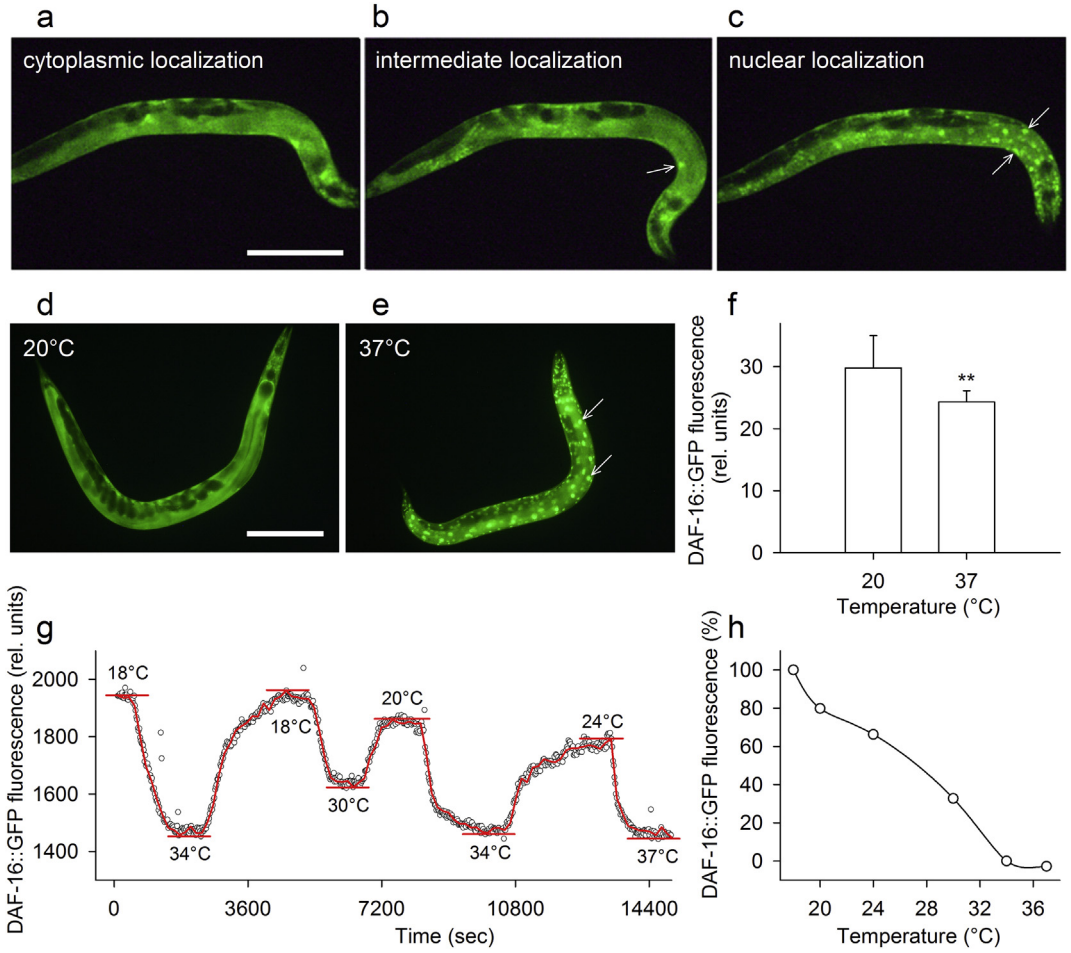

Fig. 1. Temperature and DAF-16::GFP subcellular localization. Fluorescence images (λ_{ex} = 460 nm, λ_{em} > 520 nm) of a DAF-16::GFP-expressing *C. elegans* TJ356 worm showing (a) a predominantly cytoplasmic, (b) an intermediate, or (c) a predominately nuclear localization of the reporter construct at 20 °C, 30 °C, or 37 °C. The increases in DAF-16::GFP nuclear occupancy between (d) 20 °C and (e) 37 °C caused (f) a significant reduction in the DAF-16::GFP fluorescence intensity of whole worms (mean ± SD, N = 9 worms each; $^{**}P \leq 0.01$, unpaired t-test), which was determined with ImageJ [26] using the digital information of the 18 images. (g) Incremental changes in temperature (mostly between 18 °C and 34 °C) caused reversible changes in the DAF-16::GFP fluorescence intensity (λ_{ex} = 460 nm, λ_{em} > 520 nm) of a group of TJ356 worms (N = 150–200 synchronized adult worms) within a small droplet of M9 buffer, which was recorded using a photomultiplier (red curves resulted from local data smoothing, and horizontal lines mark local minima/maxima). (h) After data normalization (see text), characteristic curves were derived from (g) the measured changes in fluorescence intensity. The white arrows indicate a nuclear localization of DAF-16::GFP, and the white bars correspond to a length of 200 µm. (For interpretation of the references to colour in this figure legend, the reader is referred to the web version of this article.)

the housekeeping gene *cdc-42* [29].

2.8. Statistical analyses and graphs

Data represent the mean ± standard deviation (SD) or mean ± standard error (SE), with n indicating the number of experiments and N the number of worms. One-, two- or three-way analyses of variance (ANOVA) and a subsequent multiple comparison procedure (HOLM-SIDAK analysis) or unpaired t-tests were used to test for differences between curves or single mean values. SigmaPlot 11.0 (Systat Software, Erkrath, Germany) was used for graph preparations and statistical analyses.

3. Results

3.1. Effects of temperature on the subcellular localization of DAF-16::GFP

The subcellular localization of DAF-16::GFP and other reporter protein-coupled TFs has hitherto been evaluated by microscopic examination and qualitative categorization (e.g. cytoplasmic, intermediate, or nuclear localization) (Fig. 1a-c). We detected that the large-scale nuclear translocation of DAF-16::GFP molecules in the *C. elegans* strain TJ356 between 20 °C (Fig. 1d) and 37 °C (Fig. 1e) caused a significant reduction in the DAF-16::GFP fluorescence intensity of whole worms (Fig. 1f). This effect can be explained by self absorption and quenching, resulting from the accumulation and higher concentration of the numerous DAF-16::GFP fluorophores of a worm in the smaller scaled nuclear compartments (see Discussion). This effect provides the opportunity to assess the cytoplasmic-nuclear shuttling of DAF-16::GFP under changing ambient conditions in a quantitative and time-resolved manner. Actually, we determined reversible and reproducible decreases and increases in the DAF-16::GFP fluorescence intensity of 150–200 TJ356 worms within a small droplet of buffer due to incremental changes in ambient temperature (Fig. 1g). To level out variations in absolute fluorescence intensity between experiments due to variations in worm number and/or slight drifts, the experimental protocol included repeated measurements at minimal and maximal ambient conditions (e.g. 18 °C and 34 °C) to normalize the intermediate data in relation to the data at the extremes (e.g. data at 18 °C ≙ 100% and data at 34 °C ≙ 0%). In this way, characteristic curves between the environmental factor (e.g. temperature) and the DAF-16::GFP fluorescence intensity of whole worms were created (Fig. 1h). The 'temperature characteristic' showed a largely linear decrease in DAF-16::GFP

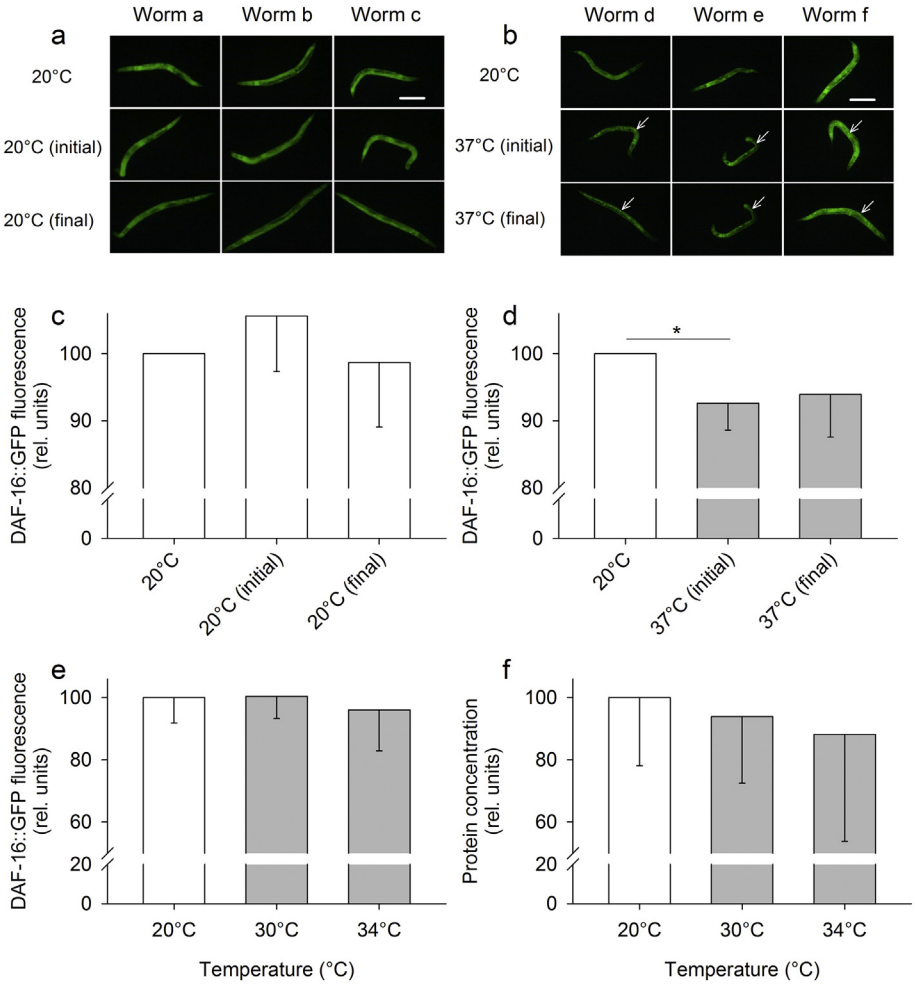

Fig. 2. The heat-induced decreases in DAF-16::GFP fluorescence intensity were not due to lowered DAF-16::GFP concentrations. Control experiments excluded that the decreases in DAF-16::GFP fluorescence intensity at 34 °C (see Fig. 1g) were due to protein degradation. Fluorescence images (λ_{ex} = 460 nm, λ_{em} > 520 nm) were taken of (a, b, top) six living TJ356 worms at 20 °C (white bars: 200 µm) and of the same worms (a, b, centre) after 10-min incubations at 20 °C or 37 °C, temporary freezing and thawing and (a, b, bottom) after another 30 min at 20 °C. (a, b, top) Living or (a, centre, bottom) dead worms that were permanently kept at 20 °C showed a predominantly cytoplasmic localization of DAF-16::GFP. (b, centre, bottom) The heat-exposed worms, however, showed, even after their death due to freezing, a strongly nuclear localization of DAF-16::GFP (white arrows). The DAF-16::GFP fluorescence intensity of these worms was determined using ImageJ [26], and the data were normalized (living worms: 100%) and averaged. The mean DAF-16::GFP fluorescence intensity showed (c) no significant changes at 20 °C but (d) a significant decrease after heat exposure (mean ± SD, $N = 3$ worms each; $^{*}P \leq 0.05$, unpaired *t*-test). Thus, short-term heat exposure induced a higher nuclear localization and lower fluorescence intensity of DAF-16::GFP. In a next experimental series, batches of several hundred synchronized adult TJ356 worms were incubated for 30 min at 20 °C, 30 °C, or 34 °C. After freezing and thawing, the DAF-16::GFP fluorescence intensity (λ_{ex} = 460 nm, λ_{em} > 520 nm) and protein concentration of these samples were measured, and the data were normalized (20 °C-incubated worms: 100%) and averaged. The mean (e) DAF-16::GFP fluorescence intensity and (f) protein concentration did not significantly differ between the three incubation temperatures (mean ± SD, $n = 16$ biological replicates per temperature condition). Thus, short-term heat exposure did not induce changes in DAF-16::GFP concentration.

fluorescence intensity (i.e. increase in DAF-16::GFP nuclear occupancy) with rising temperature.

Control experiments were carried out to exclude that the decrease in DAF-16::GFP fluorescence intensity with rising temperature was due to a decrease in DAF-16::GFP concentration (e.g. heat-induced protein degradation). First, images were taken of the DAF-16::GFP fluorescence of (i) six living TJ356 worms (at 20 °C) and of these worms (ii) after a 10-min period at 20 °C or 37 °C, freezing (at −80 °C) and thawing (at 20 °C), and (iii) after another 30 min at room temperature (20 °C). DAF-16::GFP showed a predominantly cytoplasmic localization in living or dead worms that were never exposed to 37 °C (Fig. 2a and 2b, top). Incubations at 37 °C, however, caused a strongly nuclear localization of DAF-16::GFP which persisted in dead animals (Fig. 2b, centre, bottom). Thus, freezing fixed the DAF-16::GFP subcellular localization. Incubations at 20 °C did not significantly alter the DAF-16::GFP fluorescence intensity of these worms (Fig. 2c). Incubations at 37 °C, however, caused a significant drop in the DAF-16::GFP fluorescence intensity which also persisted in dead animals (Fig. 2d). These results show once again that DAF-16::GFP nuclear localization led to a reduced DAF-16::GFP fluorescence intensity. Next, we applied a similar experimental protocol (30-min incubations at 20 °C, 30 °C, or 34 °C, freezing and thawing) to samples of many hundred worms, with soluble proteins then extracted for subsequent measurements, which showed no significant differences in DAF-16::GFP fluorescence intensity (Fig. 2e) or protein concentration (Fig. 2f) between the three different incubation temperatures. Thus, the concentration of DAF-16::GFP was not significantly affected by short-term exposures to 30 °C or 34 °C, even if a slight decrease in protein concentration may have occurred during heat exposure.

3.2. *Effects of oxygen partial pressure on the subcellular localization of DAF-16::GFP*

As central experiment of this study, we applied incremental changes in oxygen partial pressure (Po_2) between 0 and 20.4 kPa and measured again reversible and reproducible decreases and increases in the DAF-16::GFP fluorescence intensity of 150–200 TJ356 worms within a small droplet of buffer (Fig. 3a). The corresponding characteristic curve ('Po_2 characteristic') exhibited a non-linear decrease in DAF-16::GFP fluorescence intensity (i.e. increase in DAF-16::GFP nuclear occupancy) with decreasing Po_2, with an initially moderate decrease followed by a strong decrease at low Po_2 (Fig. 3b).

As previous studies reported a reversible red shift of GFP fluorescence emission under hypoxic conditions as consequence of a preceding photoactivation with blue light [30,31], control experiments were carried out to rule out this effect in our experiments. We applied the standard Po_2-protocol (Fig. 3a) and measured the fluorescence emission of 150–200 TJ356 worms both in the "green" and "red" spectral range. The "green" fluorescence emission proved to be several times higher than the "red" fluorescence emission (Fig. 3c), and the patterns of changes in fluorescence emission were identical in both spectral ranges, particularly at hypoxic Po_2 values (Fig. 3d, e). Thus, a reversible red shift of GFP fluorescence emission during hypoxia can be excluded in our experiments. To rule out contributions by other fluorophores (i.e.

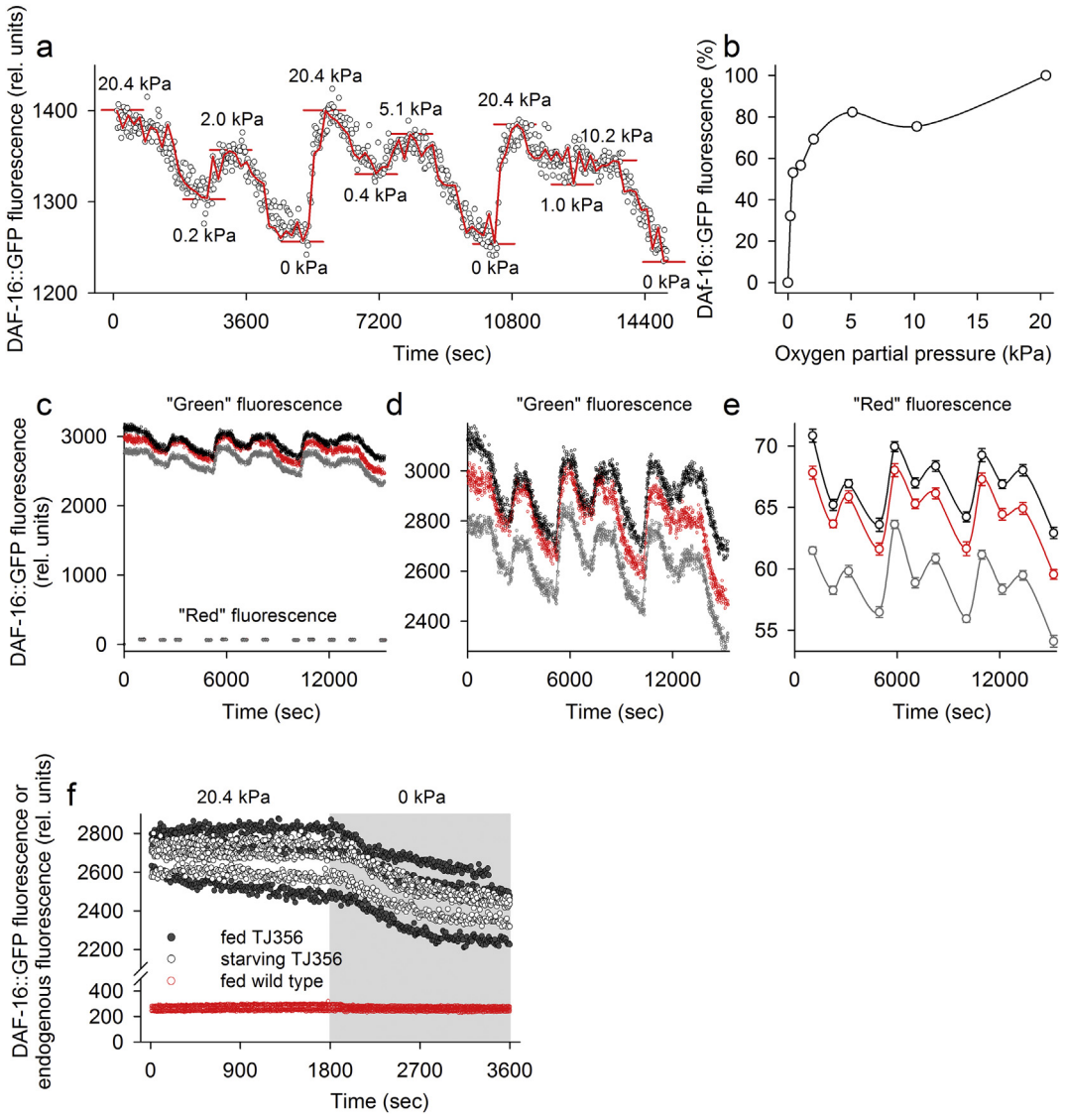

Fig. 3. Oxygen partial pressure and DAF-16::GFP subcellular localization. (a) Incremental changes in oxygen partial pressure (Po_2; 0–20.4 kPa) caused reversible changes in the DAF-16::GFP fluorescence intensity (λ_{ex} = 460 nm, λ_{em} > 520 nm) of a group of TJ356 worms (N = 150–200 synchronized adult worms) within a small droplet of M9 buffer, which was recorded using a photomultiplier (red curves resulted from local data smoothing, and horizontal lines mark local minima/maxima). (b) After data normalization (see text), characteristic curves were derived from (a) the measured changes in fluorescence intensity. (c–e) Control experiments excluded that the Po_2-specific changes in DAF-16::GFP fluorescence intensity were due to red-shifted GFP fluorescence emission under hypoxic conditions [30,31]. Applying the standard Po_2-protocol (a), the fluorescence emission of 150–200 synchronized adult TJ356 worms was measured three times (black, red, and gray traces) both in the "green" (λ_{ex} = 460 nm, λ_{em} > 520 nm) and "red" (λ_{ex} = 460 nm, λ_{em} > 590 nm) spectral range, with filter changes to measure the "red" fluorescence emission only performed when local minima/maxima were reached. These experiments excluded a red-shifted GFP fluorescence emission at hypoxic Po_2 values, (i) because (c) the "green" fluorescence emission exceeded the "red" fluorescence emission by orders of magnitude and (ii) because the patterns of changes in fluorescence emission were identical in the (d) "green" (single values and smoothed curves) and (e) "red" (mean ± SD) spectral range. (f) Other control experiments excluded significant contributions by bacterial or endogenous fluorescence to (a) the measured changes in DAF-16::GFP fluorescence intensity, (i) because the fluorescence intensity and its changes during normoxia (Po_2 = 20.4 kPa) and subsequent anoxia (0 kPa) were not systematically linked to the presence or absence of bacterial feed (*E. coli* OP50) during experiments (fed or starving TJ356 worms; n = 3 or 4 experiments on N = 150–200 synchronized adult worms each) and (ii) because the endogenous fluorescence intensity of fed (*E. coli* OP50) wild type was several times lower and independent of the ambient Po_2 (n = 4 experiments on N = 150–200 synchronized adult worms each). (For interpretation of the references to colour in this figure legend, the reader is referred to the web version of this article.)

bacterial fluorophores or endogenous fluorophores of *C. elegans*) to the measured changes in fluorescence intensity (Fig. 3a), we determined the DAF-16::GFP fluorescence intensity of 150–200 fed or starving TJ356 worms and of 150–200 fed wild type (WT) worms during normoxia and subsequent anoxia (Fig. 3f). As the nutritional status of the TJ356 worms did not affect absolute fluorescence intensities and their changes, significant contributions by bacterial fluorescence can be excluded. Much lower fluorescence intensities in WT than in TJ356 and the absence of intensity changes in WT excluded contributions by endogenous fluorescence. As the WT worms were fed with bacteria, significant contributions by bacterial fluorescence to the DAF-16::GFP fluorescence can be ruled out once again.

3.3. Hypoxia promotes DAF-16::GFP nuclear occupancy

The mean Po_2 characteristic of TJ356 control worms (Fig. 4a) showed similarity with the Po_2-specific aerobic metabolic rate of this species (i.e. the rate of carbon dioxide production; [32]), with a strong

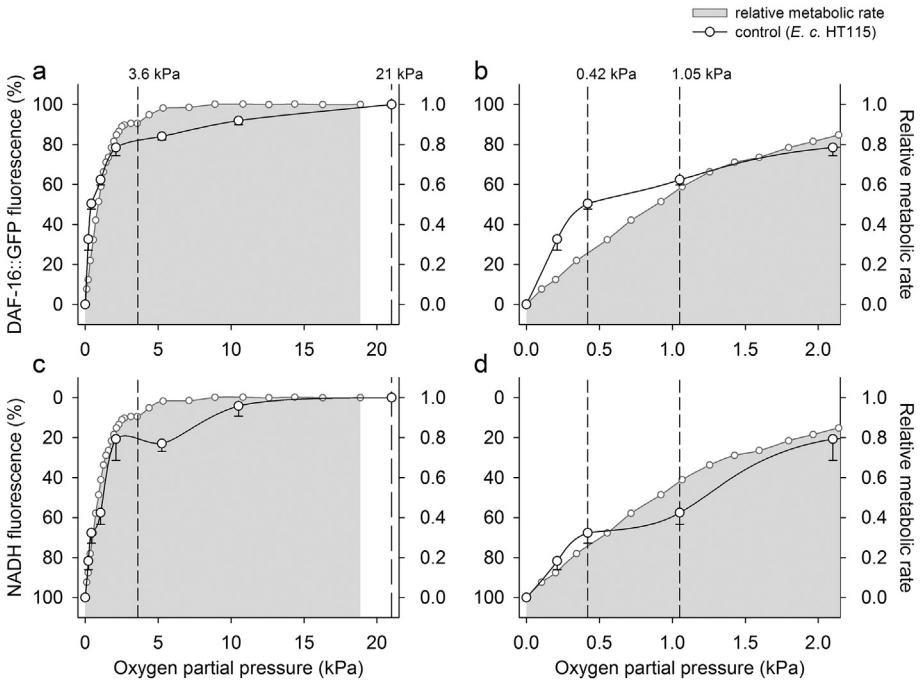

Fig. 4. Po_2 characteristic and Po_2-specific NADH fluorescence. (a, b) The Po_2 characteristic (λ_{ex} = 460 nm, λ_{em} > 520 nm) and (c, d) the Po_2-specific endogenous NADH fluorescence intensity (λ_{ex} = 350 nm, λ_{em} > 420 nm; please note the inverse scaling) of TJ356 control worms that were fed with *E. coli* HT115 are depicted (a, c) over the whole Po_2 range (0–21 kPa) or (b, d) only between 0 and 2.15 kPa (mean ± SE; per type of fluorescence measurement, n = 6–8 experiments on N = 150–200 synchronized adult worms each) (left y-axes). Light gray areas show the Po_2-specific aerobic metabolic rate of wild type (right y-axes) [32]. The critical Po_2 (P_cO_2 = 3.6 kPa) and normoxia ($Po_2 \approx$ 21 kPa) are indicated by dashed vertical lines. Note the smaller changes in DAF-16::GFP and NADH fluorescence intensity between 0.42 and 1.05 kPa.

increase in DAF-16::GFP nuclear occupancy or decrease in metabolic rate slightly below the critical Po_2 (P_cO_2 = 3.6 kPa in *C. elegans* [32]), which marks the onset of anaerobic metabolism. In comparison with the aerobic metabolic rate, the mean Po_2 characteristic showed only slight changes between 0.42 and 1.05 kPa, but a sharp increase in DAF-16::GFP nuclear occupancy at Po_2 values below 0.42 kPa (Fig. 4b). To enable a comparison between the Po_2 characteristic and the mitochondrial oxidation-reduction state, the endogenous NADH fluorescence, which primarily originates from mitochondrial protein-bound NADH (binding of NADH to complex I; see Discussion), was measured at changing Po_2 from 150 to 200 TJ356 worms within a small droplet of buffer. These data were also normalized in relation to the values at 0 (≙ 100%) and 20.4 kPa (≙ 0%) (Fig. 4c; please note the inverse Y-axis scaling). In contrast to the Po_2 characteristic, the mean NADH fluorescence intensity increased with decreasing Po_2, particularly below the P_cO_2, indicating an increasingly reduced mitochondrial state (i.e. a higher level of complex I-bound NADH), and it also showed only slight changes between 0.42 and 1.05 kPa, but a sharp increase at Po_2 values below 0.42 kPa (Fig. 4d).

3.4. H_2O_2 (ROS) promotes DAF-16::GFP nuclear occupancy

To assess the effects of different H_2O_2 (ROS) concentrations on the Po_2 characteristic, TJ356 control worms were exposed to 0, 0.02, or 1 mmol/L of H_2O_2 during measurements, which caused rightward shifts of the mean Po_2 characteristics (i.e. higher P_cO_2 values) with increasing H_2O_2 concentration (Fig. 5). Thus, strong increases in DAF-16::GFP nuclear occupancy were shifted to ever higher Po_2 values.

3.5. *aak-2(RNAi)* promotes DAF-16::GFP nuclear occupancy and *let-363(RNAi)* affects the Po_2-specific NADH fluorescence

In comparison with the mean Po_2 characteristic of TJ356 control worms, *aak-2(RNAi)* caused a significant increase in DAF-16::GFP nuclear occupancy at Po_2 values above the P_cO_2 (Fig. 6a). The mean Po_2 characteristics of the *aak-2(RNAi)*- or *let-363(RNAi)*-treated TJ356 worms again showed only slight changes in DAF-16::GFP nuclear occupancy between 0.42 and 1.05 kPa, but sharp increases at Po_2 values below 0.42 kPa (Fig. 6b, f). In comparison with the mean Po_2-specific

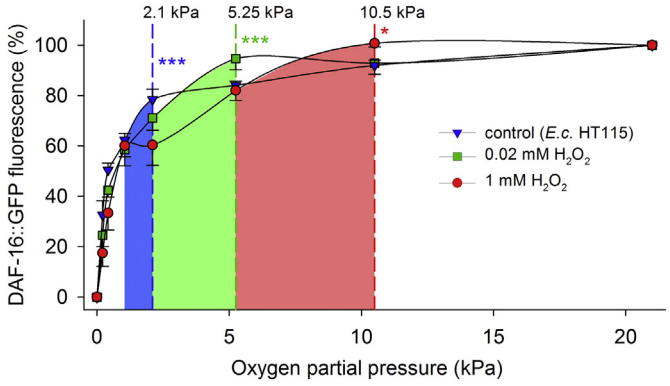

Fig. 5. Effects of different H_2O_2 (ROS) concentrations on the Po_2 characteristic. The Po_2 characteristic (λ_{ex} = 460 nm, λ_{em} > 520 nm) of TJ356 control worms was determined during exposures to 0 (blue triangles), 0.02 (green squares), or 1 mmol/L of H_2O_2 (red circles) (mean ± SE; per H_2O_2 concentration, n = 5–6 experiments on N = 150–200 synchronized adult worms each). Asterisks indicate the statistical significance (one-way ANOVA and subsequent HOLM-SIDAK analysis) of differences in DAF-16::GFP fluorescence intensity at Po_2 values of 2.1, 5.25, or 10.5 kPa and the next smaller Po_2 value (indicated by blue, green, or red area fill colours): $^{*}P \leq 0.05$ or $^{***}P \leq 0.001$, with even higher significance levels at still lower Po_2 values. (For interpretation of the references to colour in this figure legend, the reader is referred to the web version of this article.)

NADH fluorescence of TJ356 control worms, *aak-2(RNAi)* had no significant effect on this relationship (Fig. 6c, d). *let-363(RNAi)*, however, caused a significant decrease in NADH fluorescence intensity (i.e. a highly oxidized mitochondrial state) at a Po_2 of 10.5 kPa, which was even below the level under normoxia (Fig. 6g). The mean Po_2-specific NADH fluorescence intensities of the *aak-2(RNAi)*- or *let-363(RNAi)*-treated TJ356 worms also showed only slight changes between 0.42 and 1.05 kPa but sharp increases at Po_2 values below 0.42 kPa (Fig. 6d, h), with the NADH fluorescence of *let-363(RNAi)*-treated worms even reaching a maximal level under severe hypoxia (Fig. 6h)

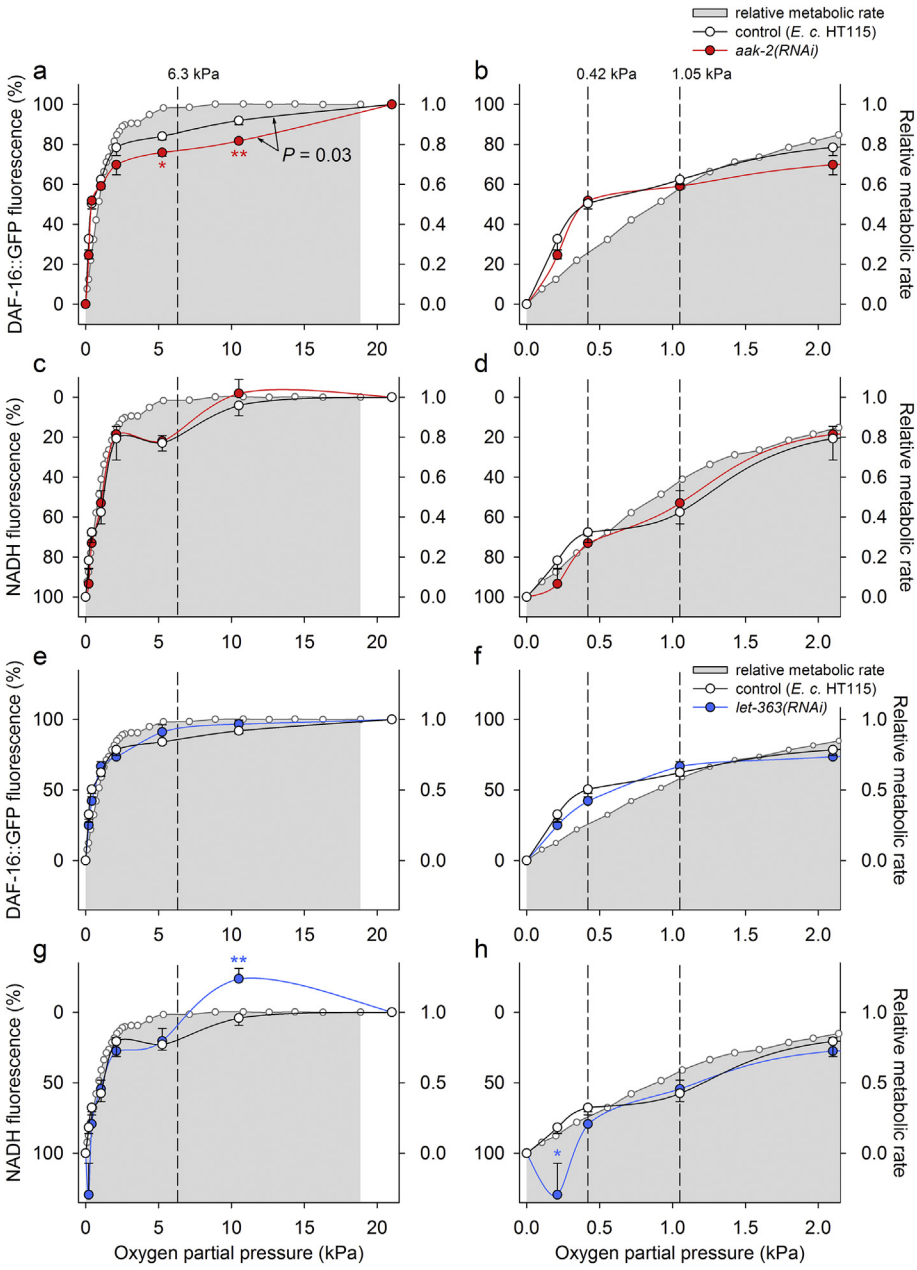

Fig. 6. Effects of *aak-2(RNAi)* and *let-363(RNAi)* on the Po_2 characteristic and Po_2-specific NADH fluorescence. (a–b, e–f) The Po_2 characteristic (λ_{ex} = 460 nm, λ_{em} > 520 nm) and (c–d, g–h) the Po_2-specific endogenous NADH fluorescence intensity (λ_{ex} = 350 nm, λ_{em} > 420 nm; please note the inverse scaling) of (a–d) *aak-2(RNAi)*-treated (red circles) or (e–h) *let-363(RNAi)*-treated (blue circles) TJ356 worms and (a–h) TJ356 control worms (white circles) are depicted (a, c, e, g) over the whole Po_2 range (0–21 kPa) or (b, d, f, h) only between 0 and 2.15 kPa (mean ± SE; per type of treatment and fluorescence measurement, n = 4–7 experiments on N = 150–200 synchronized adult worms each) (left y-axes). Significant differences were detected by (a) two-way ANOVA and subsequent HOLM-SIDAK analysis (P = 0.03) or (a, g, h) unpaired t-tests ($^{*}P \leq 0.05$, $^{**}P \leq 0.01$). Light gray areas show the Po_2-specific aerobic metabolic rate of wild type (right y-axes) [32]. The hypoxic Po_2 (6.3 kPa) later applied during mRNA expression measurements (see Fig. 8) is indicated by a dashed vertical line. Note the smaller changes in DAF-16::GFP and NADH fluorescence intensity between 0.42 and 1.05 kPa. (For interpretation of the references to colour in this figure legend, the reader is referred to the web version of this article.)

3.6. aak-2(RNAi) accelerates and let-363(RNAi) decelerates the developmental speed of TJ356 worms under hypoxia and normoxia

To ensure that *aak-2(RNAi)* and *let-363(RNAi)* were effective and affect anabolic processes (Fig. 6), the developmental speed from egg to adult worm, which was considered as an indicator of anabolic activity, was determined in *aak-2(RNAi)*- or *let-363(RNAi)*-treated TJ356 worms and in TJ356 control worms under moderate hypoxia (Po_2 = 6.3 kPa) or normoxia ($Po_2 \approx$ 21 kPa). Developmental speed differed significantly between hypoxia and normoxia under all experimental conditions (Fig. 7), with a higher percentage of adult worms under hypoxia than under normoxia during late development (between 86 and 96 h). *aak-2(RNAi)*-treated worms reached adulthood significantly faster (Fig. 7a, d) and *let-363(RNAi)*-treated worms significantly slower (Fig. 7c, f) than control worms (Fig. 7b, e) both under hypoxia and normoxia. Thus, *aak-2(RNAi)* accelerated and *let-363(RNAi)* decelerated the developmental speed (i.e. anabolic activity) of these worms.

3.7. aak-2(RNAi) promotes mRNA expression of the DAF-16 target gene sod-3 under hypoxia and normoxia

To validate the higher DAF-16::GFP nuclear occupancy in *aak-2(RNAi)*-treated TJ356 worms at Po_2 values above the P_co_2 (Fig. 6a), RT-qPCR was used to measure the mRNA expression of the well-known DAF-16 target gene *sod-3* [18] in TJ356 worms that were kept either for 3 h under moderate hypoxia (Po_2 = 6.3 kPa) or permanently under normoxia. After hypoxia (Fig. 8a) and during normoxia (Fig. 8b), *aak-2(RNAi)* caused a significantly higher *sod-3* mRNA expression in comparison to that in TJ356 control worms, whereas *let-363(RNAi)* showed no significant effects ($P \geq 0.18$).

4. Discussion

4.1. Quantification of the relationships between environmental factors and DAF-16::GFP subcellular localization

The subcellular localization of DAF-16::GFP and other reporter

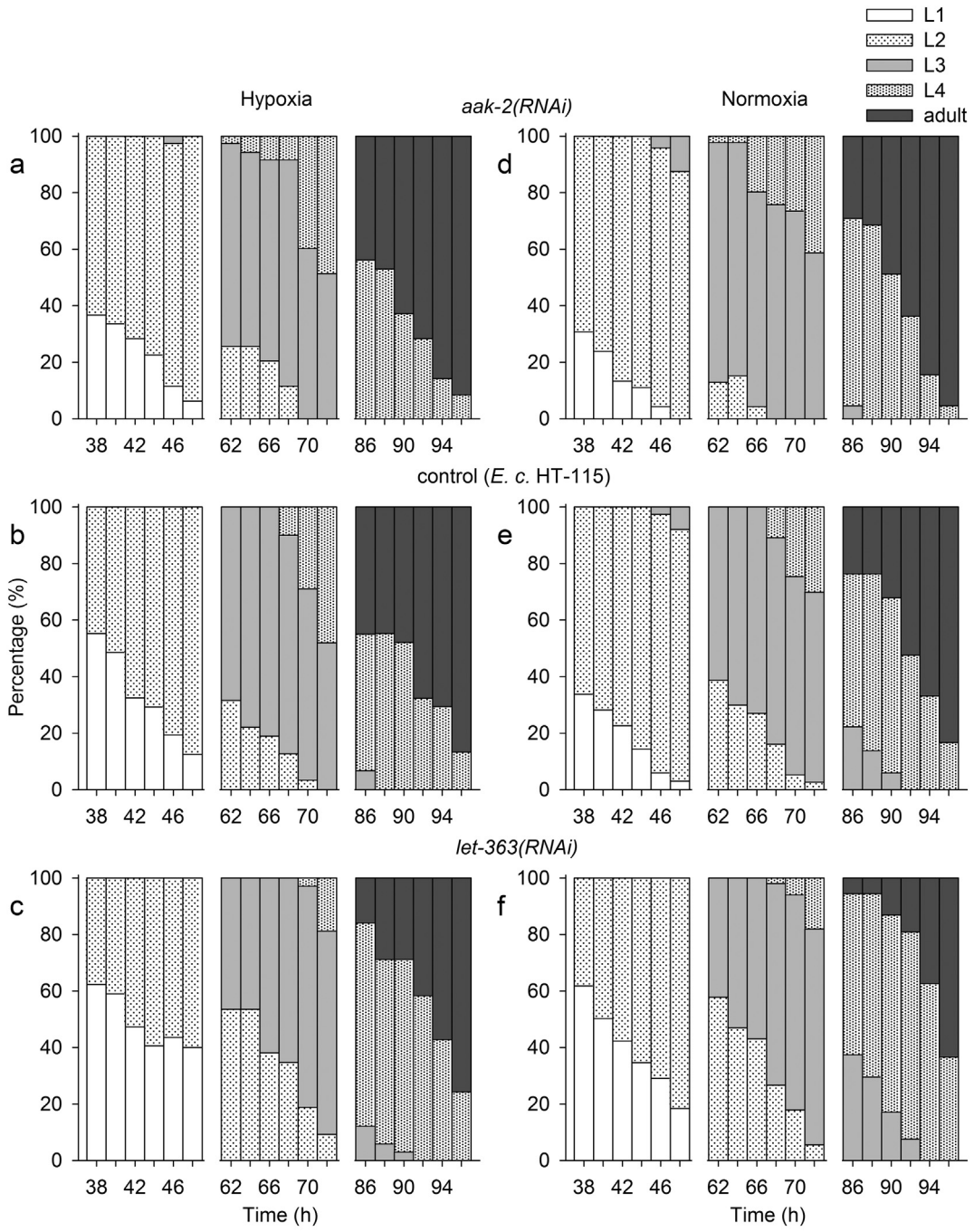

Contrast	L1	L2	L3	L4	Adult
hypoxia vs. normoxia	$P < 0.001$	$P = 0.003$	$P = 0.001$	$P = 0.033$	$P < 0.001$
aak-2(RNAi) vs. control	$P = 0.005$	-	-	-	$P < 0.001$
aak-2(RNAi) vs. *let-363(RNAi)*	$P < 0.001$	-	-	-	$P < 0.001$
control vs. *let-363(RNAi)*	$P < 0.001$	-	-	-	$P < 0.001$

Fig. 7. Effects of *aak-2(RNAi)* and *let-363(RNAi)* on developmental speed. The developmental speed of (a, d) *aak-2(RNAi)*-treated or (c, f) *let-363(RNAi)*-treated TJ356 worms and (b, e) TJ356 control worms was assessed under (a–c) hypoxia (Po_2 = 6.3 kPa) or (d–f) normoxia ($Po_2 \approx$ 21 kPa) by determining the percentages of L1, L2, L3, L4 larvae and adult worms over time (zero is the point in time at the end of egg laying). Data are mean values of two independent experimental series for each of the six conditions (two Po_2 values and three RNAi treatments) on N = 12–25 worms per experimental series. Significant differences in developmental speed were detected between hypoxia and normoxia and among the three different experimental conditions in case of L1 larvae and adult worms (P values from three-way ANOVA and subsequent HOLM-SIDAK analysis).

protein-coupled TFs has hitherto been assessed by microscopic examination and qualitative categorization (e.g. cytoplasmic, intermediate, or nuclear localization) (Fig. 1a-c). The new finding that the large-scale cytoplasmic-nuclear shuttling of DAF-16::GFP molecules (Fig. 1d, e) causes changes in the total fluorescence intensity of whole animals (Fig. 1f) opens up the possibility to determine the relationships between environmental factors (e.g. temperature, Po_2) and the subcellular localization of reporter-coupled TFs in a quantitative and time-

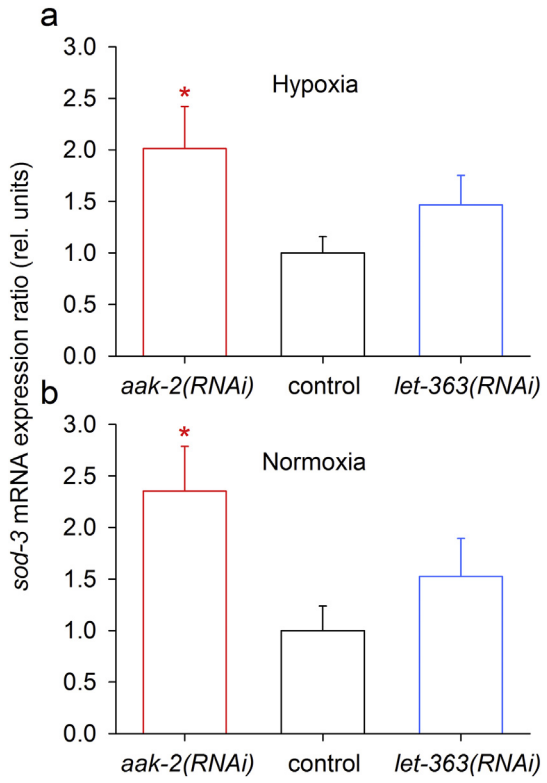

Fig. 8. Effects of *aak-2(RNAi)* on the mRNA expression of the DAF-16 target gene *sod-3*. Expression of the DAF-16 target gene *sod-3* (superoxide dismutase 3) was measured on the mRNA level (expression ratio, with *cdc-42* mRNA as reference) in *aak-2(RNAi)*-treated or *let-363(RNAi)*-treated TJ356 worms and TJ356 control worms under (a) hypoxia (Po_2 = 6.3 kPa) or (b) normoxia ($Po_2 \approx$ 21 kPa) (mean ± SE; per type of treatment and Po_2 condition, n = 8–9 experiments on several hundred synchronized adult worms each). Asterisks indicate significant differences ($^*P \leq 0.05$; unpaired *t*-tests).

resolved manner. Prerequisites for the use of this new method are transparency of the organism, strong fluorescence intensities of the reporter-coupled TFs, and synchronous transports of them between the cytoplasmic and nuclear compartments under the influence of environmental changes. The changes in total fluorescence intensity (Fig. 1f) are likely related to unequal volumes of the cytoplasmic and nuclear spaces of an animal (i.e. more wide-lumened cytoplasmic and rather narrow-lumened nuclear spaces). The mass transport of the numerous reporter-coupled TFs of an animal from the cytoplasmic to the nuclear compartments is thus likely to rise the nuclear GFP concentration to a level where self absorption and fluorescence quenching takes place [33], with the consequence of a reduced fluorescence emission of the worms. From the environment-induced changes in DAF-16::GFP fluorescence intensity (Fig. 1g, 3a), characteristic curves between the environmental factor and the corresponding fluorescence intensity (i.e. DAF-16::GFP subcellular localization) were derived after data normalization (Figs. 1h, 3b).

Control experiments for this new approach included short-term exposures to high temperature to exclude DAF-16::GFP degradation during experiments (Fig. 2). As the reproductive fitness of the worms is maximum under hypoxia (Po_2 = 3.6 kPa, [34]), and as their well-developed anaerobic metabolism allows them to survive anoxia for several hours [35], the experiments with varying Po_2, on which this study focused (Figs. 3–8), were certainly less stressful than the short-term exposures to heat. Thus, DAF-16::GFP degradation was also highly unlikely in case of the short-term exposures to hypoxia or anoxia. Moreover, the initially fast decreases in fluorescence intensity at high temperatures (34 °C; Fig. 1g) or low Po_2 values (0 kPa; Fig. 3a) or increases at low temperatures (18 °C) or high Po_2 values (20.4 kPa) were followed by largely stable fluorescence intensities after about 30 min. The stabilized fluorescence levels as well as the similar size of the decreases and subsequent increases in DAF-16::GFP fluorescence intensity also rule out significant DAF-16::GFP degradation during experiments. The reversibility and equal size of the fluorescence changes additionally exclude DAF-16::GFP denaturation as this would have significantly reduced transfers through the nuclear pore complexes. Additional control experiments (Fig. 3) excluded effects of hypoxia on the fluorescence properties of GFP (i.e. red-shifted GFP fluorescence emission [30,31]), or significant contributions by bacterial or endogenous fluorescence to the measured DAF-16::GFP fluorescence intensities.

4.2. Po_2 characteristic and Po_2-specific NADH fluorescence

The Po_2 characteristic of TJ356 control worms (Fig. 4a, b) showed similarity with the Po_2-specific aerobic metabolic rate of *C. elegans* [32], where a critical Po_2 (P_cO_2 [36]) of 3.6 kPa separates two Po_2 ranges with a predominant use of different types of energy (ATP) generation. Aerobic metabolism prevails under 'moderate hypoxia' ($Po_2 > P_cO_2$) and anaerobic metabolism increasingly replaces aerobic energy provision under 'severe hypoxia' ($Po_2 < P_cO_2$). Additionally, one should distinguish between 'hypoxia' (i.e. an ambient Po_2 below the normoxic Po_2) and 'tissue hypoxia' (i.e. a lowered tissue Po_2), which is especially important in case of *C. elegans* as the shape of the Po_2-specific aerobic metabolic rate of these tiny worms results from the balance between diffusive oxygen supply and metabolic energy demand. Thus, tissue hypoxia and anaerobic energy provision only arise under severe hypoxia, whereas diffusive oxygen supply is sufficient to support aerobic metabolism under moderate hypoxia. The strongly decreasing DAF-16::GFP fluorescence intensity during severe hypoxia (Fig. 4a) was interrupted by a less steep curve progression at Po_2 values between 0.42 and 1.05 kPa (Fig. 4b), which will be discussed later.

The Po_2-specific changes in endogenous NADH fluorescence intensity (Fig. 4c, d) mainly resulted from varying levels of NADH bound to complex I (mitochondrial NADH dehydrogenase) [37,38], with a higher fluorescence intensity corresponding to a more reduced state of mitochondria (i.e. higher level of complex I-bound NADH) and a lower fluorescence intensity to a more oxidized state. Thus, the increase in NADH fluorescence intensity during severe hypoxia resulted from an accumulation of NADH at complex I, which was caused by significant increases in the cytoplasmic production and level of NADH due to accelerated anaerobic glycolysis and decelerated mitochondrial electron transports at decreasing Po_2. The strongly increasing NADH fluorescence intensity during severe hypoxia (Fig. 4c) was also interrupted by a less steep curve progression at Po_2 values between 0.42 and 1.05 kPa (Fig. 4d). The rising cytoplasmic use of NADH for the production of anaerobic end products (e.g. lactate) may have attenuated the cytoplasmic-mitochondrial flux of NADH, with the consequence of smaller changes in the mitochondrial redox state. The simultaneously rising anaerobic ATP production may have compensated, at least in part, for the decrease in aerobic ATP production, with the possible effect that the AMP:ATP ratio also changed to a lesser extent between 0.42 and 1.05 kPa.

4.3. Reasons for the Po_2-specific changes in DAF-16::GFP nuclear occupancy

Several signals are known, which may have determined the Po_2 characteristic of TJ356 control worms (Fig. 4a, b). These signals include reactive oxygen species (ROS), higher AMPK activity, and elevated NAD^+ levels. In animal tissues, ROS are primarily produced within mitochondria [39]. There is also evidence that the redox state of the electron transport chain affects mitochondrial ROS production [40], which severely increases during tissue hypoxia [41–43]. ROS may promote DAF-16 nuclear occupancy in several ways. Elevated ROS levels activate the neuronal MAP kinase JNK-1 of *C. elegans*, which

promotes DAF-16 nuclear occupancy either directly in neuronal cells [44] or indirectly in peripheral cells [45]. Other stress-responsive protein kinases may additionally control DAF-16 nuclear occupancy [46]. A ROS-induced disulfide formation of DAF-16 with the nuclear import receptor transportin-1 is also necessary for DAF-16 nuclear translocation due to ROS [47]. Another reaction chain linking ROS and DAF-16 nuclear translocation may start with an activation of AMPK by ROS [48]. As activated AMPK inhibits TORC1 signalling [5], the TORC1-dependent inhibition of DAF-16 activity [21] may be cancelled. AMPK activation may additionally result from an increasing AMP:ATP ratio during tissue hypoxia. The NAD^+ level may also affect DAF-16 nuclear translocation, which involves sirtuin (Sir) activity. Increasing NAD^+ levels promote DAF-16 nuclear occupancy, for instance, in dependence on Sir-2.1 activity [49], and Sir-2.4 promotes DAF-16 nuclear occupancy in response to stress [50].

Evidence for ROS-induced DAF-16::GFP nuclear translocations during tissue hypoxia came from experiments on the effects of H_2O_2 on the Po_2 characteristic of TJ356 control worms (Fig. 5), which showed that strong and significant increases in DAF-16::GFP nuclear occupancy were shifted to ever higher Po_2 values (below 2.1, 5.25, and 10.5 kPa) with rising H_2O_2 concentration (0, 0.02, and 1 mmol/L of H_2O_2). Internally produced ROS due to tissue hypoxia and externally applied ROS (H_2O_2) that diffused into the cells likely added up to an elevated internal ROS level, which induced DAF-16::GFP nuclear translocation at ever higher Po_2 values. Minor changes in the mitochondrial redox state (Fig. 4d) and hence mitochondrial ROS production [40] at Po_2 values between 0.42 and 1.05 kPa could also explain the reduced increase in DAF-16::GFP nuclear occupancy in this Po_2 range (Fig. 4b). Elevated NAD^+ levels as reason for the strong increase in DAF-16::GFP nuclear occupancy during severe hypoxia can be excluded because the NADH level increased and the NAD^+ level decreased at Po_2 values below the P_cO_2 (Fig. 4c, d). Thus, ROS and/or higher AMPK activity are remaining signals for the determination of the Po_2 characteristic.

4.4. Effects of aak-2(RNAi) and let-363(RNAi) on the Po_2 characteristic and Po_2-specific NADH fluorescence

Experiments on the developmental speed of TJ356 worms showed that *aak-2(RNAi)* accelerated and *let-363(RNAi)* decelerated anabolic activity both under moderate hypoxia and normoxia (Fig. 7), with the higher anabolic activity under moderate hypoxia probably related to the greater reproductive fitness of the worms under this environmental condition [34]. *aak-2(RNAi)* promoted anabolic activity by reducing the negative effects of AMPK (AAK-2) activity on TORC1 (LET-363) signalling and anabolic processes [51–53]. *let-363(RNAi)* diminished anabolic activity by reducing TORC1 signalling, which, however, was certainly not completely efficient as the worms developed to the adult stage [54]. *aak-2(RNAi)* and *let-363(RNAi)* also affected the Po_2 characteristic and/or the Po_2-specific NADH fluorescence of TJ356 worms. *aak-2(RNAi)* induced a significantly higher DAF-16::GFP nuclear occupancy (Fig. 6a), and *let-363(RNAi)* led to a significantly higher NAD^+ level (i.e. lower NADH level) (Fig. 6g) under moderate hypoxia. The higher DAF-16::GFP nuclear occupancy due to *aak-2(RNAi)* was additionally verified by a significantly higher mRNA expression of the DAF-16 target gene *sod-3* under moderate hypoxia and normoxia (Fig. 8). As the DAF-16::GFP fluorescence intensity under normoxic conditions ($Po_2 \approx 21$ kPa) was set to 100% during data normalization (see Results), the corresponding Po_2 characteristic (Fig. 6a), however, did not show a lowered DAF-16::GFP fluorescence intensity at this Po_2 value.

These experiments (Fig. 6) excluded activated AMPK and/or inhibited TORC1 signalling as well as again elevated NAD^+ levels as reasons for a higher DAF-16::GFP nuclear occupancy. Increased AMPK activity and/or decreased TORC1 signalling can be excluded as signals, because reduced AMPK activity due to *aak-2(RNAi)* even promoted DAF-16::GFP nuclear occupancy (Fig. 6a), and reduced TORC1 activity due to *let-363(RNAi)* did not affect the Po_2 characteristic (Fig. 6e). Elevated NAD^+ levels as signal can again be ruled out, because the NAD^+ (NADH) levels were similar in TJ356 control and *aak-2(RNAi)*-treated worms (Fig. 6c) but their Po_2 characteristics differed (Fig. 6a), and the NAD^+ (NADH) levels differed in TJ356 control and *let-363(RNAi)*-treated worms (Fig. 6g) but their Po_2 characteristics were similar (Fig. 6e). Thus, the measured Po_2 characteristics were most likely determined by ROS as signal.

The higher DAF-16::GFP nuclear occupancy due to *aak-2(RNAi)* (Fig. 6a), which took place at a sufficient supply of oxygen (i.e. under moderate hypoxia), cannot be explained by tissue hypoxia and a higher production and level of ROS. The absent effects of *aak-2(RNAi)* on the Po_2-specific NADH fluorescence (Fig. 6c) also speak against a mitochondrial production of ROS under moderate hypoxia. Previous studies on *Drosophila* and mammalian cells, however, have shown that TORC1 activation increases ROS production [55–57]. Thus, the increased TORC1 activity due to *aak-2(RNAi)* (Fig. 7) could have caused an elevated ROS production under moderate hypoxia, with the effect that the nuclear occupancy of DAF-16::GFP increased. Decreased TORC1 activity due to *let-363(RNAi)*, in turn, may explain the higher NAD^+ level under moderate hypoxia (Fig. 6g). As the ATP demand for protein biosynthesis, which uses up to 40% of total ATP [58], and other anabolic processes was likely to be considerably reduced in the *let-363(RNAi)*-treated worms, a resultant surplus of ATP may have led to the well-known ATP-mediated allosteric inhibition of catabolic pathways and NADH production [59], with the consequence of lower NADH and higher NAD^+ levels.

5. Conclusions

Using a newly developed method, the relationships between Po_2 and DAF-16::GFP subcellular localization were quantified in the *C. elegans* strain TJ356 under control conditions as well as under the influence of ROS or upon RNAi treatment and analysed and compared with the relationships between Po_2 and mitochondrial redox state (NADH fluorescence). Taking into account different Po_2-related signals, the data provide evidence that increases in the production and level of ROS induced the measured increases in DAF-16::GFP nuclear occupancy under tissue hypoxia or due to *aak-2(RNAi)* under moderate hypoxia. Thus, metabolic conditions, which lead to higher ROS levels, seem to induce countermeasures in the form of DAF-16-mediated stress gene expression. Future perspectives of the novel method may include (i) evaluation of the temporal information in the data (i.e. nuclear entry or exit times of TFs), (ii) analysis of the relationships between environmental factors and other fluorescence-labelled TFs, or (iii) additional RNAi treatments to downregulate signalling pathways, which affect the cytoplasmic-nuclear shuttling of a specific TF.

Ethics approval

According to German law, experiments involving the invertebrate *C. elegans* do not have to be announced or approved.

Consent for publication

Not applicable.

Availability of data and material

The data supporting the conclusions of this article are included within the article.

Competing interests

The authors declare that they have no competing interests.

Funding

This study was supported by the Deutsche Forschungsgemeinschaft (DFG grant Pa 308/13-1).

Authors' contributions

T.S., S.A.W., and R.J.P. performed the design study; M.N.M., A.K., and N.H. carried out the test realization; M.N.M. and R.J.P. performed the data analysis; M.N.M. and R.J.P. carried out the data interpretation; and M.N.M. and R.J.P. created the manuscript. All authors read and approved the final manuscript.

Acknowledgements

We particularly thank Norman Post, as well as Thorben Rötting, Fynn Krause, and Jens Kleinehr, for their contributions during methodical development.

References

[1] A. Salminen, K. Kaarniranta, AMP-activated protein kinase (AMPK) controls the aging process via an integrated signaling network, Ageing Res. Rev. 11 (2012) 230–241, https://doi.org/10.1016/j.arr.2011.12.005.
[2] J. Apfeld, G. O'Connor, T. McDonagh, P.S. DiStefano, R. Curtis, The AMP-activated protein kinase AAK-2 links energy levels and insulin-like signals to lifespan in *C. elegans*, Genes Dev. 18 (2004) 3004–3009, https://doi.org/10.1101/gad.1255404.
[3] B.B. Kahn, T. Alquier, D. Carling, D.G. Hardie, AMP-activated protein kinase: ancient energy gauge provides clues to modern understanding of metabolism, Cell Metab. 1 (2005) 15–25, https://doi.org/10.1016/j.cmet.2004.12.003.
[4] G. Thomas, D.M. Sabatini, M.N. Hall, TOR: Target of Rapamycin, Springer, Berlin, Heidelberg, New York, 2004 ISBN: 978-3-642-18930-2.
[5] S. Wullschleger, R. Loewith, M.N. Hall, TOR signaling in growth and metabolism, Cell 124 (2006) 471–484, https://doi.org/10.1016/j.cell.2006.01.016.
[6] C. Selman, J.M.A. Tullet, D. Wieser, E. Irvine, S.J. Lingard, A.I. Choudhury, et al., Ribosomal protein S6 kinase 1 signaling regulates mammalian lifespan, Science 326 (2009) 140–144, https://doi.org/10.1126/science.1177221.
[7] M. Barbieri, M. Bonafè, C. Franceschi, G. Paolisso, Insulin/IGF-I-signaling pathway: an evolutionarily conserved mechanism of longevity from yeast to humans, Am. J. Physiol. Endocrinol. Metab. 285 (2003) E1064–E1071, https://doi.org/10.1152/ajpendo.00296.2003.
[8] S.D. Narasimhan, K. Yen, H.A. Tissenbaum, Converging pathways in lifespan regulation, Curr. Biol. 19 (2009) R657–R666, https://doi.org/10.1016/j.cub.2009.06.013.
[9] G.A. Kleemann, C.T. Murphy, The endocrine regulation of aging in *Caenorhabditis elegans*, Mol. Cell. Endocrinol. 299 (2009) 51–57, https://doi.org/10.1016/j.mce.2008.07.005.
[10] K. Yen, S.D. Narasimhan, H.A. Tissenbaum, DAF-16/Forkhead Box O transcription factor: many paths to a single Fork(head) in the road, Antioxid. Redox Signal. 14 (2011) 623–634, https://doi.org/10.1089/ars.2010.3490.
[11] S.T. Henderson, T.E. Johnson, *daf-16* integrates developmental and environmental inputs to mediate aging in the nematode *Caenorhabditis elegans*, Curr. Biol. 11 (2001) 1975–1980, https://doi.org/10.1016/S0960-9822(01)00594-2.
[12] S.F. Leiser, M. Fletcher, A. Begun, M. Kaeberlein, Life-span extension from hypoxia in *Caenorhabditis elegans* requires both HIF-1 and DAF-16 and is antagonized by SKN-1, J. Gerontol. A Biol. Sci. Med. Sci. 68 (2013) 1135–1144, https://doi.org/10.1093/gerona/glt016.
[13] L. Tao, Q. Xie, Y.H. Ding, S.T. Li, S. Peng, Y.P. Zhang, et al., CAMKII and calcineurin regulate the lifespan of *Caenorhabditis elegans* through the FOXO transcription factor DAF-16, eLife 2 (2013) e00518, , https://doi.org/10.7554/eLife.00518.
[14] J.H. An, T.K. Blackwell, SKN-1 links *C. elegans* mesendodermal specification to a conserved oxidative stress response, Genes Dev. 17 (2003) 1882–1893, https://doi.org/10.1101/gad.1107803.
[15] C.T. Murphy, The search for DAF-16/FOXO transcriptional targets: approaches and discoveries, Exp. Gerontol. 41 (2006) 910–921, https://doi.org/10.1016/j.exger.2006.06.040.
[16] Y. Honda, S. Honda, The *daf-2* gene network for longevity regulates oxidative stress resistance and Mn-superoxide dismutase gene expression in *Caenorhabditis elegans*, FASEB J. 13 (1999) 1385–1393 PMID: 10428762.
[17] K. Jia, D. Chen, D.L. Riddle, The TOR pathway interacts with the insulin signaling pathway to regulate *C. elegans* larval development, metabolism and life span, Development 131 (2004) 3897–3906, https://doi.org/10.1242/dev.01255.
[18] C.T. Murphy, S.A. McCarroll, C.I. Bargmann, A. Fraser, R.S. Kamath, J. Ahringer, et al., Genes that act downstream of DAF-16 to influence the lifespan of *Caenorhabditis elegans*, Nature 424 (2003) 277–283, https://doi.org/10.1038/nature01789.
[19] E.L. Greer, D. Dowlatshahi, M.R. Banko, J. Villen, K. Hoang, D. Blanchard, et al., An AMPK-FOXO pathway mediates longevity induced by a novel method of dietary restriction in *C. elegans*, Curr. Biol. 17 (2007) 1646–1656, https://doi.org/10.1016/j.cub.2007.08.047.
[20] E.L. Greer, P.R. Oskoui, M.R. Banko, J.M. Maniar, M.P. Gygi, S.P. Gygi, et al., The energy sensor AMP-activated protein kinase directly regulates the mammalian FOXO3 transcription factor, J. Biol. Chem. 282 (2007) 30107–30119, https://doi.org/10.1074/jbc.M705325200.
[21] S. Robida-Stubbs, K. Glover-Cutter, D.W. Lamming, M. Mizunuma, S.D. Narasimhan, E. Neumann-Haefelin, et al., TOR signaling and rapamycin influence longevity by regulating SKN-1/Nrf and DAF-16/FoxO, Cell Metab. 15 (2012) 713–724, https://doi.org/10.1016/j.cmet.2012.04.007.
[22] J. Sulston, J. Hodgkin, Methods, in: W.B. Wood (Ed.), The Nematode *Caenorhabditis elegans*, CSHL Press, Cold Spring Harbor, NY, USA, 1988, pp. 587–606 ISBN: 978-087969433-3.
[23] T. Stiernagle, Maintenance of *C. elegans*, in: Research Community (Ed.), The *C. elegans*, WormBook, 2006, , https://doi.org/10.1895/wormbook.1.101.1 http://www.wormbook.org.
[24] R.J. Paul, M. Colmorgen, S. Hüller, F. Tyroller, D. Zinkler, Circulation and respiratory control in millimeter-sized animals (*Daphnia magna*, *Folsomia candida*) studied by optical methods, J. Comp. Physiol. B. 167 (1997) 399–408, https://doi.org/10.1007/s003600050089.
[25] R. Pirow, C. Bäumer, R.J. Paul, Benefits of haemoglobin in the cladoceran crustacean *Daphnia magna*, J. Exp. Biol. 204 (2001) 3425–3441 (PMID: 11707494).
[26] W.S. Rasband, ImageJ, Bethesda, Maryland, USA, U. S. National Institutes of Health, 1997https://imagej.nih.gov/ij/.
[27] M.M. Bradford, A rapid and sensitive method for the quantitation of microgram quantities of protein utilizing the principle of protein-dye binding, Anal. Biochem. 72 (1976) 248–254, https://doi.org/10.1016/0003-2697(76)90527-3.
[28] O.J. Marshall, PerlPrimer: cross-platform, graphical primer design for standard, bisulphite and real-time PCR, Bioinformatics 20 (2004) 2471–2472, https://doi.org/10.1093/bioinformatics/bth254.
[29] D. Hoogewijs, K. Houthoofd, F. Matthijssens, J. Vandesompele, J.R. Vanfleteren, Selection and validation of a set of reliable reference genes for quantitative *sod* gene expression analysis in *C. elegans*, BMC Mol. Biol. 9 (2008) 9, , https://doi.org/10.1186/1471-2199-9-9.
[30] M.B. Elowitz, M.G. Surette, P.E. Wolf, J. Stock, S. Leibler, Photoactivation turns green fluorescent protein red, Curr. Biol. 7 (1997) 809–812, https://doi.org/10.1016/S0960-9822(06)00342-3.
[31] E. Takahashi, T. Takano, Y. Nomura, S. Okano, O. Nakajima, M. Sato, In vivo oxygen imaging using green fluorescent protein, Am. J. Physiol. Cell Physiol. 291 (2006) C781–C787, https://doi.org/10.1152/ajpcell.00067.2006.
[32] W.A. Van Voorhies, S. Ward, Broad oxygen tolerance in the nematode *Caenorhabditis elegans*, J. Exp. Biol. 203 (2000) 2467–2478 (PMID: 10903161).
[33] G. Henderson, The effects of absorption and self-absorption quenching on fluorescent intensities, J. Chem. Educ. 54 (1977) 57–59, https://doi.org/10.1021/ed054p57.
[34] K. Freyth, T. Janowitz, F. Nunes, M. Voss, A. Heinick, J. Bertaux, et al., Reproductive fitness and dietary choice behavior of the genetic model organism *Caenorhabditis elegans* under semi-natural conditions, Mol. Cells 30 (2010) 347–353, https://doi.org/10.1007/s10059-010-0125-9.
[35] R.L. Föll, A. Pleyers, G.J. Lewandovski, C. Wermter, V. Hegemann, R.J. Paul, Anaerobiosis in the nematode *Caenorhabditis elegans*, Comp. Biochem. Physiol. B Biochem. Mol. Biol. 124 (1999) 269–280, https://doi.org/10.1016/S0305-0491(99)00130-3.
[36] H.O. Pörtner, M.K. Grieshaber, Critical Po_2(s) in oxyconforming and oxyregulating animals: gas exchange, metabolic rate and the mode of energy production, in: J.E.P.W. Bicudo (Ed.), The Vertebrate Gas Transport Cascade: Adaptations to Environment and Mode of Life, CRC Press, Boca Raton, FL, USA, 1993, pp. 330–357.
[37] M. Wakita, G. Nishimura, M. Tamura, Some characteristics of the fluorescence lifetime of reduced pyridine nucleotides in isolated mitochondria, isolated hepatocytes and perfused rat liver in situ, J. Biochem. 118 (1995) 1151–1160 PMID: 8720129.
[38] R.J. Paul, J. Gohla, R. Föll, H. Schneckenburger, Metabolic adaptations to environmental changes in *Caenorhabditis elegans*, Comp. Biochem. Physiol. B Biochem. Mol. Biol. 127 (2000) 469–479 PMID: 11281264.
[39] J.F. Turrens, Mitochondrial formation of reactive oxygen species, J. Physiol. 552 (2003) 335–344, https://doi.org/10.1113/jphysiol.2003.049478.
[40] N.D. Bonawitz, M. Chatenay-Lapointe, Y. Pan, G.S. Shadel, Reduced TOR signaling extends chronological life span via increased respiration and upregulation of mitochondrial gene expression, Cell Metab. 5 (2007) 265–277, https://doi.org/10.1016/j.cmet.2007.02.009.
[41] N.S. Chandel, E. Maltepe, E. Goldwasser, C.E. Mathieu, M.C. Simon, P.T. Schumacker, Mitochondrial reactive oxygen species trigger hypoxia-induced transcription, Proc. Natl. Acad. Sci. U. S. A. 95 (1998) 11715–11720 PMCID: PMC21706.
[42] R.D. Guzy, P.T. Schumacker, Oxygen sensing by mitochondria at complex III: the paradox of increased reactive oxygen species during hypoxia, Exp. Physiol. 91 (2006) 807–819, https://doi.org/10.1113/expphysiol.2006.033506.
[43] C.T. Taylor, Mitochondria and cellular oxygen sensing in the HIF pathway, Biochem. J. 409 (2008) 19–26, https://doi.org/10.1042/BJ20071249.
[44] S.W. Oh, A. Mukhopadhyay, N. Svrzikapa, F. Jiang, R.J. Davis, H.A. Tissenbaum, JNK regulates lifespan in Caenorhabditis elegans by modulating nuclear translocation of forkhead transcription factor/DAF-16, Proc. Natl. Acad. Sci. U. S. A. 102 (2005) 4494–4499, https://doi.org/10.1073/pnas.0500749102.
[45] M. Wolf, F. Nunes, A. Henkel, A. Heinick, R.J. Paul, The MAP kinase JNK-1 of *Caenorhabditis elegans*: location, activation, and influences over temperature-dependent insulin-like signaling, stress responses, and fitness, J. Cell. Physiol. 214 (2008) 721–729, https://doi.org/10.1002/jcp.21269.

[46] L.O. Klotz, C. Sánchez-Ramos, I. Prieto-Arroyo, P. Urbánek, H. Steinbrenner, M. Monsalve, Redox regulation of FoxO transcription factors, Redox Biol. 6 (2015) 51–72, https://doi.org/10.1016/j.redox.2015.06.019.
[47] M. Putker, T. Madl, H.R. Vos, H. de Ruiter, M. Visscher, M.C.W. van den Berg, et al., Redox-dependent control of FOXO/DAF-16 by transportin-1, Mol. Cell 49 (2013) 730–742, https://doi.org/10.1016/j.molcel.2012.12.014.
[48] P.T. Mungai, G.B. Waypa, A. Jairaman, M. Prakriya, D. Dokic, M.K. Ball, et al., Hypoxia triggers AMPK activation through reactive oxygen species-mediated activation of calcium release-activated calcium channels, Mol. Cell. Biol. 31 (2011) 3531–3545, https://doi.org/10.1128/MCB.05124-11.
[49] L. Mouchiroud, R.H. Houtkooper, N. Moullan, E. Katsyuba, D. Ryu, C. Cantó, et al., The NAD(+)/sirtuin pathway modulates longevity through activation of mitochondrial UPR and FOXO signaling, Cell 154 (2013) 430–441, https://doi.org/10.1016/j.cell.2013.06.016.
[50] W.C. Chiang, D.X. Tishkoff, B. Yang, J. Wilson-Grady, X. Yu, T. Mazer, et al., *C. elegans* SIRT6/7 homolog SIR-2.4 promotes DAF-16 relocalization and function during stress, PLoS Genet. 8 (2012) e1002948, , https://doi.org/10.1371/journal.pgen.1002948.
[51] D.G. Hardie, AMPK - sensing energy while talking to other signaling pathways, Cell Metab. 20 (2014) 939–952, https://doi.org/10.1016/j.cmet.2014.09.013.
[52] D.G. Hardie, M.L. Ashford, AMPK: regulating energy balance at the cellular and whole body levels, Physiology (Bethesda) 29 (2014) 99–107, https://doi.org/10.1152/physiol.00050.2013.
[53] R.C. Russell, H.X. Yuan, K.L. Guan, Autophagy regulation by nutrient signaling, Cell Res. 24 (2014) 42–57, https://doi.org/10.1038/cr.2013.166.
[54] X. Long, C. Spycher, Z. Stanley Han, A.M. Rose, F. Müller, J. Avruch, TOR deficiency in *C. elegans* causes developmental arrest and intestinal atrophy by inhibition of mRNA translation, Curr. Biol. 12 (2002) 1448–1461, https://doi.org/10.1016/S0960-9822(02)01091-6.
[55] M.J. Tuñón, S. Sánchez-Campos, B. Gutiérrez, J.M. Culebras, J. González-Gallego, Effects of FK506 and rapamycin on generation of reactive oxygen species, nitric oxide production and nuclear factor kappa B activation in rat hepatocytes, Biochem. Pharmacol. 66 (2003) 439–445 (PMID: 12907243).
[56] J.H. Kim, S.C. Chu, J.L. Gramlich, Y.B. Pride, E. Babendreier, D. Chauhan, et al., Activation of the PI3K/mTOR pathway by BCR-ABL contributes to increased production of reactive oxygen species, Blood 105 (2005) 1717–1723, https://doi.org/10.1182/blood-2004-03-0849.
[57] J.H. Lee, A.V. Budanov, E.J. Park, R. Birse, T.E. Kim, G.A. Perkins, et al., Sestrin as a feedback inhibitor of TOR that prevents age-related pathologies, Science 327 (2010) 1223–1228, https://doi.org/10.1126/science.1182228.
[58] F. Buttgereit, M.D. Brand, A hierarchy of ATP-consuming processes in mammalian cells, Biochem. J. 312 (1995) 163–167 (PMCID: PMC1136240).
[59] P.W. Hochachka, G.N. Somero, Biochemical Adaptation, University Press, Princeton, NJ, USA, 1984 ISBN: 978-1-4008-5541-4.